JOURNAL OF THE ROYAL SOCIETY Interface

CrossMark click for updates

J. R. Soc. Interface (2012) **9**, 3260–3267
doi:10.1098/rsif.2012.0527
Published online 29 August 2012

Embodied linearity of speed control in *Drosophila melanogaster*

V. Medici[1,*] and S. N. Fry[1,2]

[1]*Institute of Neuroinformatics, University of Zurich and ETH Zurich, Winterthurerstrasse 190, 8057 Zurich, Switzerland*
[2]*SciTrackS GmbH, Lohzelgstrasse 7, 8118 Pfaffhausen, Switzerland*

Fruitflies regulate flight speed by adjusting their body angle. To understand how low-level posture control serves an overall linear visual speed control strategy, we visually induced free-flight acceleration responses in a wind tunnel and measured the body kinematics using high-speed videography. Subsequently, we reverse engineered the transfer function mapping body pitch angle onto flight speed. A linear model is able to reproduce the behavioural data with good accuracy. Our results show that linearity in speed control is realized already at the level of body posture-mediated speed control and is therefore embodied at the level of the complex aerodynamic mechanisms of body and wings. Together with previous results, this study reveals the existence of a linear hierarchical control strategy, which can provide relevant control principles for biomimetic implementations, such as autonomous flying micro air vehicles.

Keywords: *Drosophila melanogaster*; insect flight; behaviour; flight control; aerodynamics

1. INTRODUCTION

Fruitflies, like many other insects, control their ground speed from the visually perceived motion of objects passing by (optic flow) (for reviews, see [1,2]). Because these reflexive speed responses are highly stereotyped and easily elicited in freely flying insects, they have served as a powerful behavioural paradigm to study the underlying sensorimotor mechanisms for many decades (mosquitoes [3]; honey bees [4,5]; flies [6–9]). More recently, the visuomotor control mechanisms underlying flight speed responses were studied in fruitflies using a real-time controlled virtual reality (VR) environment termed *TrackFly* [8]. By presenting flies with short bouts of regressive (back-to-front) moving patterns, the backward drift an insect might visually perceive when hit by a gust of wind was simulated to elicit compensatory forward acceleration responses. These were shown to depend directly on the velocity (measured in metres per second) of the moving patterns according to an amazingly simple proportional control law [9] (likewise for lift responses see [10,11]).

The underlying physiological mechanisms that lead up to these simple control laws are complex and remain only partly understood. The principal mechanism by which a fly accelerates is to pitch its body nose down to point the flight force more forward [12,13], not unlike a helicopter. These changes in pitch are brought about by subtle changes of the wing stroke pattern, suitable to modulate pitch torque [14]. While tethered studies revealed a constant angle between the stroke-averaged flight force and the body [15], the free-flight situation manifests itself as somewhat more complex. First, the aerodynamic forces generated by the flapping wings depend on their motion relative to the surrounding air and therefore on flight speed. Second, active control of the direction of the stroke-averaged aerodynamic force vector, as recently explored in free-flight studies [16], may play an additional role.

The important role of body pitch for the control of flight speed implies the involvement of a second sensory modality, namely mechanosensory feedback from the halteres, which sense the angular velocity of the body from the resulting Coriolis forces acting on them [17,18]. Taken together, the speed control system can be conceptualized as two nested feedback control loops (figure 1). An outer speed control loop compares a set point retinal slip speed (the 'preferred' retinal slip speed [6]) with current visual input and generates as output a body pitch angle. It represents the set point pitch angle of an inner pitch control loop, which controls the body pitch angle—and hence flight speed—based on haltere signals (and possibly additional visual [19] cues).

The involvement of two sensory modalities for a stereotyped behavioural response offers a suitable model system to explore functional principles underlying multimodal flight control mechanisms. It is amenable to a behavioural system identification approach, in which the behaviour is modelled as a feedback controller [9,20–22] and the inner dynamics are subsequently 'reverse engineered' [8–11,23]. This method allows abstracting from the underlying complex physiological processes, while still capturing the fundamental high-level sensing and control principles.

*Author for correspondence (vasco@ini.phys.ethz.ch).

Electronic supplementary material is available at http://dx.doi.org/10.1098/rsif.2012.0527 or via http://rsif.royalsocietypublishing.org.

Received 4 July 2012
Accepted 3 August 2012

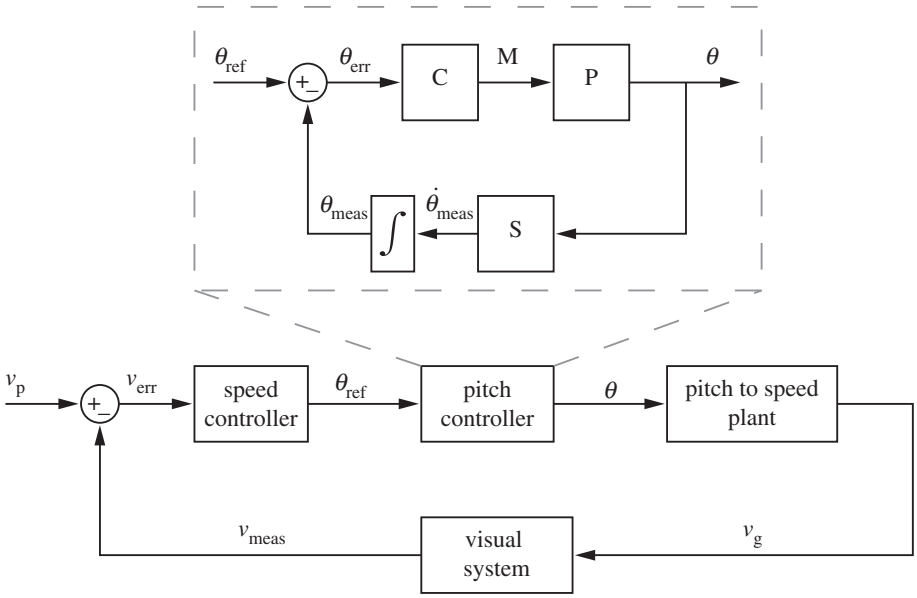

Figure 1. Hierarchical flight speed control scheme. An outer visual loop sets the desired pitch angle (θ_{ref}) according to the error between the preferred speed v_p and the measured ground speed v_g. In the inner pitch control loop (inset), the pitch controller C sets the pitch angle θ to the desired value θ_{ref} by producing a torque M around the pitch axis. P represents the plant for pitch rotation. The sensor S, representing the halteres and the visual system, measures the rotational speed $\dot{\theta}_{meas}$, which is then integrated to get the measured pitch angle θ_{meas}. The pitch angle θ is converted to v_g via the pitch-to-speed plant.

Importantly, the identification of control laws requires a quantification of a system's *plant properties*. In the case of flight speed responses, these represent the dynamics of body pitch changes and how they consequently affect flight speed. While the body pitch rotational dynamics have previously been investigated [24], the pitch-to-speed transfer function has so far not been explored in detail. The relationship between body pitch angle and flight speed has been measured only under steady-state conditions [12,13], which precludes the identification of system dynamics and consequently the description of the time course of speed responses.

Using the *TrackFly* VR set-up, we reverse engineered the dynamics of pitch-mediated speed control. We used horizontally moving visual patterns to elicit changes in horizontal flight speed of varying strength, whereas the body posture and flight speed co-varied systematically (see example in figure 3*a*(i–iii)). This approach simplified the system identification due to a reduction of the dimensionality to just 3 d.f.: body pitch angle and motion along the x–z plane. The analysis can be further simplified to 2 d.f. since the accelerations occur horizontally with no significant displacement along the vertical axis.

We measured the body kinematics of the acceleration manoeuvres using high-speed videography and reverse engineered the transfer function between pitch angle and horizontal flight speed. We show that the pitch-to-speed dynamics are well described by a first-order linear transfer function. The linearity in longitudinal speed control, which has previously been described for the outer, visual control loop [7,9], extends to body posture control and is therefore embodied in the flight motor system of the fly. This linearity results from a combination of body and wing drag, of which the second dominates.

The embodiment of linear control properties provides a key to understand how flies achieve their amazing flight control feats with comparatively limited neural circuitry. Similar hardware tuning in miniature biomimetic micro air vehicles (MAVs) may eventually provide them with supreme flight capabilities under likewise severe size and performance constraints.

2. METHODS

2.1. Animals

Fruitflies (*Drosophila melanogaster*) descending from an initial population of 200 wild caught females were reared on a standard nutritive medium under a 12 L : 12 D cycle at a room temperature of about 24°C. Two-to-five day-old flies were isolated and deprived of food, but not water, for 12–16 h preceding an experiment. Experiments were performed during the first 6 h of subjective day.

2.2. Experimental set-up

The experiments were conducted using *TrackFly*, a wind tunnel equipped with VR display technology, to which a high-speed camera filming from the side was added (figure 2). As *TrackFly* has already been described in detail in Fry *et al.* [8], we provide only an overview of the relevant system's components here.

2.2.1. Wind tunnel

The experiments were performed in an open-circuit, closed-throat wind tunnel (Engineering Laboratory Design, Inc., Lake City, MN, USA). It provided a laminar air flow in a working section built from clear acrylic (1.55 m in length and 0.3 m in height and width). For the present experiments, constant wind speeds of 0.37 and 0.74 m s^{-1} were used. At the downwind end of the tunnel, a 5 per cent water solution of vinegar was

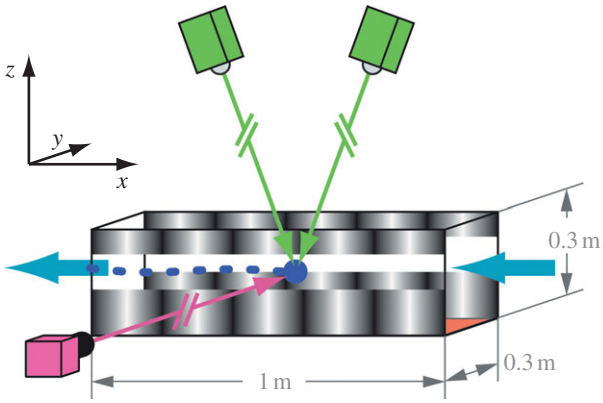

Figure 2. Schematic of the wind tunnel working section and filming system. Flies were released at the downwind end of the tunnel (left side in the figure), where they spontaneously elicited upwind flight (air flow is indicated by blue arrows). The three-dimensional position of individual flies was tracked in real time using Trackit 3D (SciTrackS GmbH, Pfaffhausen, Switzerland, cameras shown in green). The position data were used to control the speed of the visual pattern projected onto the side walls, as well as trigger a high-speed (1000 fps) recording of acceleration manoeuvres from the side (camera shown in pink). For further details on the applied methods, see Fry *et al.* [8].

vaporized at a rate of approximately 7.2 mg s^{-1} to motivate the flies to fly upwind.

2.2.2. Real-time position tracking

Trackit 3D (SciTrackS GmbH, Pfaffhausen, Switzerland [25]), a two camera (green in figure 2) three-dimensional tracking system, was used to track the position of flies in real time (latency: 38 ms) from above against a long wavelength (more than 700 nm) back lighting.

2.2.3. Image rendering and display

Custom programmed software based on the VisionEgg open-source library [26] was used to render visual stimuli consisting of vertically oriented sine gratings. The images were displayed using a 60 Hz flicker-free LCD projector (Sony, VPL-ES1, Tokyo, Japan) onto tracing paper screens attached to the side walls of the tunnel. These screens consisted of two 0.1 m vertically spaced sections (1×0.13 m and 1×0.07 m for the bottom and top screens, respectively), leaving a 0.1 m vertical slit along the length of the screen.

2.2.4. High-speed recording

To measure the body pitch angle, flies were filmed through these slits from the side using a high-speed camera (Photonfocus, MV-D1024-Trackcam, Lachen, Switzerland, in pink in figure 2). The high-speed camera was equipped with a 1024×1024 pixels CMOS image sensor and filmed the centre of the wind tunnel at 1000 frames per second (fps), with an exposure time of 50 µs and a field of view of 22.5×10 cm (approx. 14°). The high frame rate was achieved by exploiting the dynamic region of interest functionality of the camera (also see [27]).

2.3. Measurement procedure

The experiments were completely automated and consisted of a pre-test positioning phase and a testing phase. The visual stimuli consisted of horizontally moving vertically oriented sine gratings of different linear spatial frequency (SF) and temporal frequency (TF) (following the notation of Fry *et al.* [8]).

2.3.1. Positioning phase

Inspired by David's approach [6–8], we induced single flies to fly with near zero ground speed at the downwind end of the working section by automatically varying the horizontal speed of a progressive (front-to-back) moving sine grating (SF = 6.67 m^{-1}) according to the position of the fly in the tunnel. As soon as the fly was induced to hover stably near the predefined starting position, the VR system triggered a test, after which the positioning procedure was resumed.

2.3.2. Testing phase

The high-speed recording was triggered and the fly stimulated with a short presentation (less than or equal to 3 s) of a moving pattern on the side walls of the wind tunnel. The stimuli consisted of open- and closed-loop steps and open-loop sinusoidal oscillations in retinal slip speed. In the open-loop case, the visual loop was artificially opened by continuously adjusting the pattern phase according to the fly's current position along the wind tunnel using the VR software (explained in detail in Fry *et al.* [8]). Owing to the proportional dependence of acceleration on retinal slip speed [7], this procedure also provided experimental control over the strength of the resulting accelerations. Typically, the fly flew out of the field of view of the high-speed camera long before the maximum testing duration of 3 s was reached, with an average test duration of 0.50 ± 0.17 s (mean and standard deviation).

2.3.3. Body pitch angle and x–z position measurement

We implemented a template matching algorithm to measure the body pitch angle and the x–z position (cyan in figure 3*a*(i)). The algorithm was able to ignore the wings, which due to the short exposure time were sometimes clearly visible in the acquired images, depending on the stroke angle at which the frame was taken. For each measured trajectory, the template was obtained from an image, in which the wings were not visible. The absolute pitch angle of the template was calculated by extracting the orientation from the central moments of the image.

3. RESULTS

3.1. System identification of the pitch-to-speed plant

We measured a total of 284 flight trajectories, representative examples of which are shown in figure 3 (also see electronic supplementary material, movie S1). In the first example (figure 3*a*(i–iii)), the fly was stimulated with a constant, regressive retinal pattern speed, to which the fly responded with a roughly constant forward acceleration. In the second example (figure 3*b*(i–ii)), the fly was stimulated with a horizontally oscillating retinal slip speed, to which it responded with a likewise oscillating flight speed. These responses demonstrate the linear and time invariant properties previously described for speed responses [9–11].

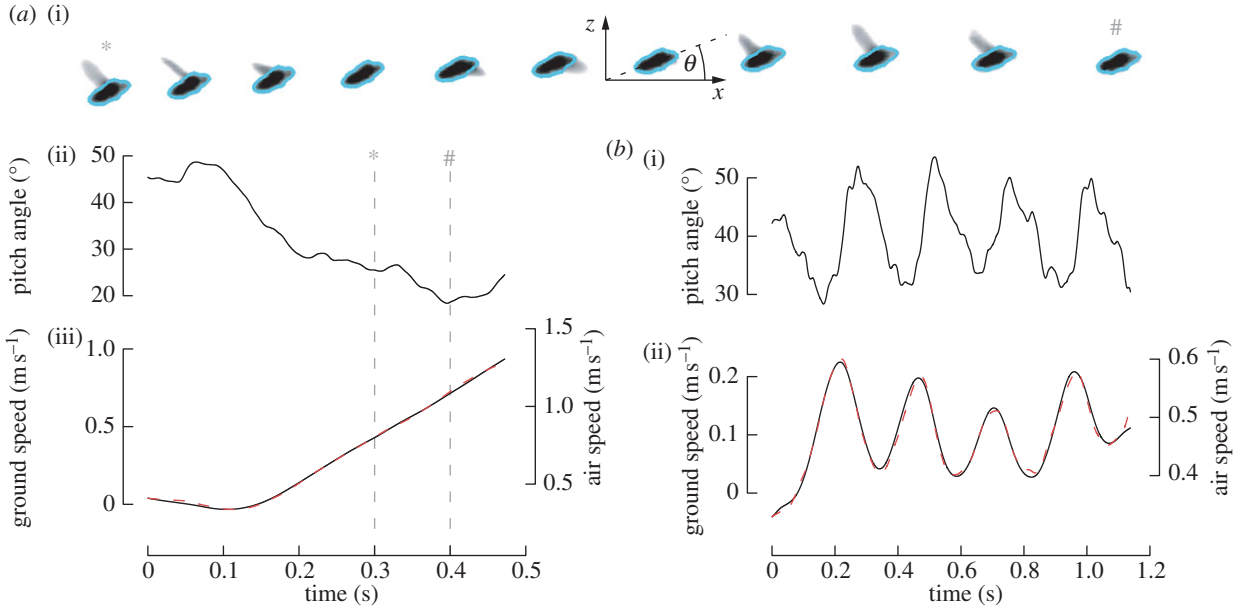

Figure 3. Behavioural measurements. (*a*) Speed response. The fly was stimulated with a sine grating that moved regressively at a constant retinal slip speed (SF = 10 m^{-1}, TF = 6 s^{-1}, wind speed WS = 0.37 m s^{-1}). (*a*(i)) High-speed camera images (down-sampled to 100 fps) filmed 300–400 ms after onset of the motion stimulus. The template matched to measure the pitch angle and position is shown in cyan. (*a*(ii)) Time course of the measured pitch angle (θ, defined in the inset of (*a*(i)), low-pass filtered with a zero-phase, fifth-order Butterworth filter with a cut-off frequency of 50 Hz). (*a*(iii)) Measured ground speed (black solid line) and linear model fitted according to equation (3.1) (red dashed line). (*b*(i),(ii)) Corresponding data for a sinusoidal modulation of retinal slip speed (SF = 6.67 m^{-1}, TF = $2.9 + 6.5 \cdot \sin(2\pi \cdot 5)$ s^{-1}, WS = 0.37 m s^{-1}).

In both examples, the body acceleration is closely correlated with body pitch angle and air speed. The flight speed can be closely fitted by a first-order linear differential equation of the form

$$\dot{v}_{\mathrm{air}} = k_0(k_1 - \theta) - k_2 v_{\mathrm{air}}, \tag{3.1}$$

where v_{air} is the fly's air speed in the x-direction, θ is the fly's body pitch angle and k_0, k_1 and k_2 are free parameters. In the case in which the fly is hovering on the spot, i.e. $v_{\mathrm{air}} = 0$ and $\dot{v}_{\mathrm{air}} = 0$, θ evaluates to k_1, which therefore represents the hovering angle. Defining $\beta = k_1 - \theta$ as the nose-down deviation of the pitch angle from the hovering pitch angle, equation (3.1) can be re-written as

$$\dot{v}_{\mathrm{air}} = k_0\beta - k_2 v_{\mathrm{air}}. \tag{3.2}$$

Assuming a constant angle between the stroke-averaged flight force and the body, β approximately describes the fly's stroke plane angle. We fitted the model of equation (3.1) to each flight trajectory using a general nonlinear optimization method (fmincon command, MATLAB, The MathWorks Inc., Natick, MA, USA) that minimized the mean quadratic error of prediction with a median R^2 of 0.997 (see two representative examples in figure 3*a*(iii) and 3*b*(ii)). We obtained the following values (median and interquartile range): $k_0 = 12.28$ [10.78 13.65] m s^{-2}, $k_1 = 0.83$ [0.78 0.89] rad and $k_2 = 4.03$ [3.03 5.22] s^{-1}. k_1 converted to degrees yields a value of 47.5°, which is close to the previously published hovering angle of *D. melanogaster* of around 45° [14]. The high R^2 of the fit shows that a simple first-order linear model suitably describes the transfer function between pitch angle and air speed. In other words, a fixed combination of pitch angle and air speed results in a constant acceleration, independent of time. This allowed us to pool all data and calculate the average horizontal acceleration as a function of pitch angle and air speed (figure 4*a*). As predicted by the linear model, the iso-response curves (representing acceleration responses of varying strength) run diagonally across the air speed–pitch angle parameter space. The flies' acceleration depends linearly on both air speed and pitch angle over the measured parameter range.

3.2. *The effect of damping on the pitch-to-speed linearity*

To understand the origin of this linearity, it is useful to consider the aerodynamic effects related to forward flapping flight. As the advance ratio (J, the ratio of body speed and mean wing tip speed) increases, the wings meet an increased air flow on the down stroke, and conversely a reduced air flow during the up stroke. This leads to a damping effect on flight speed: the so-called flapping counter force [24,28–30] (see also [31]). This phenomenon is analogous to the recently described flapping counter torque, a passive moment that develops during turning manoeuvres [32]. These effects are passive in the sense that they do not depend on changes in wing kinematics. Lacking detailed measurements of the wing kinematics, we non-specifically refer to wing damping without excluding the possibility that an active component may also be present.

To estimate wing damping, we first calculated the forward acceleration of a fly expected in the presence of body drag alone ($\hat{a}_x$). To calculate $\hat{a}_x$, we assumed a constant angle between the stroke-averaged wing force and the body, which leads to the following equation:

$$\hat{a}_x = (g + a_z - a_{\mathrm{BL}})\tan(k_1 - \theta) - a_{\mathrm{BD}}, \tag{3.3}$$

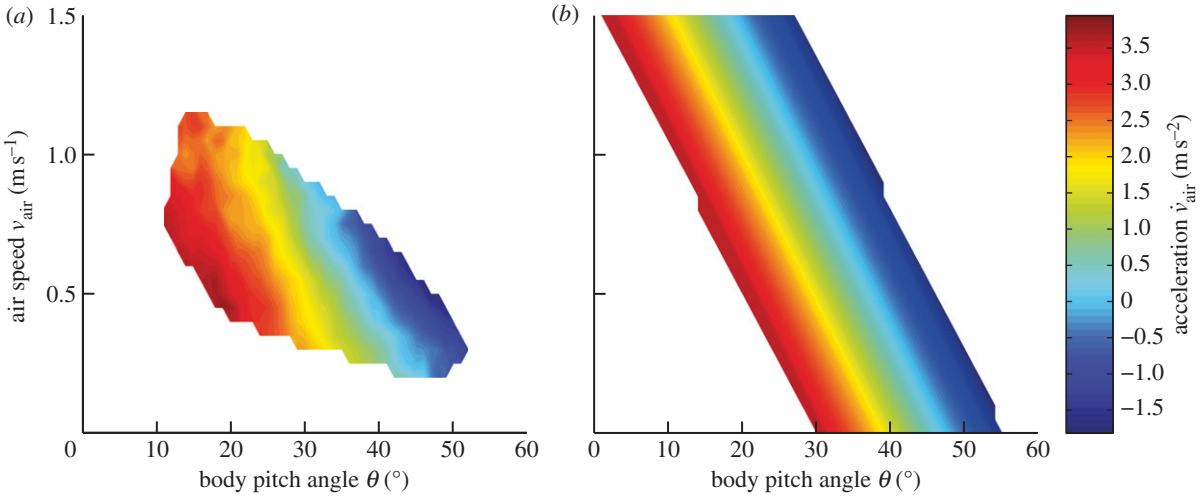

Figure 4. Acceleration responses. (*a*) Pooled behavioural data. Horizontal acceleration is plotted in colour code as a function of pitch angle and air speed. Grid size is 1° and 0.05 m s^{-1}. The figure represents a total of 284 trials, of which 191 were measured with step stimuli and 93 with sinusoidal stimuli. For each point on the grid, the median horizontal acceleration of each single measured flight trajectory was calculated by selecting the data in which the absolute vertical acceleration was smaller than 0.5 m s^{-2} (approx. 5% of the gravitational acceleration g, i.e. approx. 5% of the total vertical force) and the absolute vertical speed was smaller than 0.05 m s^{-1}. The total mean acceleration was then computed by calculating the mean of the median accelerations of the single trajectories. For a point to be valid, the data from at least six different flights were required. (*b*) Model output. Output of the fitted model based on equation (3.1).

where g is the gravitational acceleration, a_z is the measured vertical acceleration and a_{BD} and a_{BL} are the horizontal and vertical accelerations, respectively, owing to body drag. We calculated a_{BD} and a_{BL} as a function of the measured air speeds and pitch angles using a model presented by Dickson *et al.* [22] (see appendix A and electronic supplementary material, figure S1*a*,*b*). From $\hat{a}_x$, we subsequently subtracted the actual measured acceleration $a_x = \dot{v}_{air}$. The difference in acceleration can be attributed to wing damping (figure 5*a*). A comparison of the wing damping acceleration (figure 5*a*) with that due to body drag (see the electronic supplementary material, figure S1*a*) reveals a significant role of wing damping for speed control. For example, at a typical terminal speed of 0.5 m s^{-1} and a pitch angle of 38° (approx. corresponding to steady state), wing damping accounts for 88 per cent of the total braking force.

Wing damping increases monotonically with air speed and decreasing pitch angle (figure 5*a*). For typical cruising speeds below approximately 0.5 m s^{-1}, wing damping is small and covaries with air speed. At high air speeds, wing damping increases quickly as pitch angles are reduced. This effect is explained by the strongly inclined stroke plane, which is expected to lead to a roughly quadratic dependence of wing damping on air speed. While this effect causes a reduction of the total force, the fly is required to produce sufficient vertical force to offset its body weight. Taken together, it is reasonable to assume that at around $\theta = 10°$ the fruitfly reaches its locomotor limits of air speed. Indeed, in the few cases in which we observed flies pitching nose down to less than 10°, they quickly lost altitude, suggesting they were no longer able to produce sufficient lift (data not shown).

The loss of aerodynamic efficiency in the direction of flight can also be expressed in a backward tilting of the stroke-averaged force vector with respect to the body. Based on the measured body kinematics, we were able to calculate the direction of the mean force vector in the body frame of reference as a function of the pitch angle and the air speed, from

$$\gamma_{BF} = \arctan\frac{g + a_z - a_{BL}}{a_x - a_{BD}} - \theta. \qquad (3.4)$$

Because γ_{BF} varied comparatively little with respect to pitch angle (see the electronic supplementary material, figure S1*d*), we averaged the data and calculated the force angle as a function of the air speed only (figure 5*b*). We find that γ_{BF} depends roughly linearly on air speed in the measured range of 0.2–0.9 m s^{-1}, between 46° and 56°. Therefore, within the normal flight speed range of *Drosophila* ($v_{air} < 0.85$ m s^{-1} [33]), wing damping leads to a backward tilting of γ_{BF} by 15° s m^{-1}. Above 0.9 m s^{-1}, as the air speed increases γ_{BF} saturates and decreases again. This is expected because the body pitch angle is low at high air speeds and the differences between the aerodynamic forces during the up- and down-stroke are consequently small.

The combination of a high wing damping and a comparatively low body drag therefore explains the measured linearity in the pitch-to-speed transfer function.

4. DISCUSSION

4.1. Linear strategies for flight speed control

In this study, we performed a detailed behavioural and biomechanical analysis of body pitch-mediated speed control in the fruitfly. In a wind tunnel, we visually induced acceleration responses in freely flying flies, while measuring the time course of body posture and flight speed during the resulting manoeuvre. So far, the relationship between body posture and flight speed has only been measured under steady-state conditions [12,13,15], which allows predicting terminal

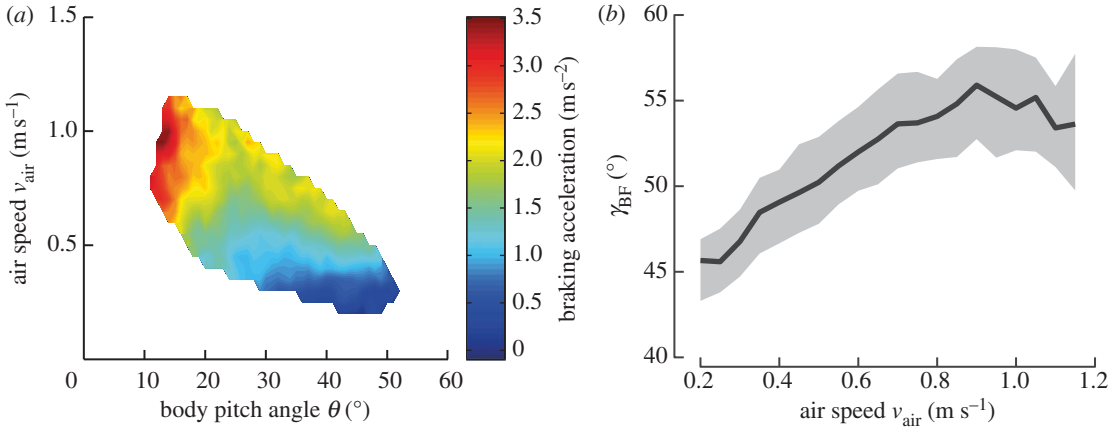

Figure 5. Effect of wing damping. (*a*) Braking acceleration owing to wing damping. Acceleration was calculated according equation (3.3), colour coded and plotted as a function of pitch angle θ and air speed v_{air}. (*b*) Stroke-averaged force angle in the body frame of reference (γ_{BF}). γ_{BF} was calculated as a function of air speed according to equation (3.4). Black line, median γ_{BF}; shaded area, γ_{BF} interquartile range.

velocities for given pitch angles. Our analysis of the time courses of pitch-dependent speed manoeuvres extends beyond previous approaches in that it provides a quantitative description of the pitch-to-speed *dynamics*, i.e. the transfer function of the plant on which the lower level neuromotor controllers act. This approach allowed us to explore the high-level control strategies on the empirical basis of measured flight speed behaviour, without making assumptions about the low-level aerodynamic mechanisms.

The pitch angle to flight speed transfer function is well described with a simple linear model (figure 4*b*). Together with the previous finding that flight speed depends linearly on pattern slip speed [9], our results lead to the conclusion that the multi-modal flight speed reflex of fruitflies is realized entirely within a linear control scheme. An interesting property of the identified linearity lies in its independence of an *absolute* reference of the pitch angle. This is because in a linear system, any given change in the sensor input leads to a given characteristic change in the output, which is independent of the absolute sensor reading. In consequence, linear controllers can operate on differential sensory input, without the need for an absolute sensor reading. The linear speed control strategy implies that flies need only to sense *changes* in pitch angle, i.e. the angular velocity of the pitching body, and not the absolute pitch angle. Such control properties are particularly relevant to animals whose sensory systems are known to signal disturbances more faithfully than absolute quantities [34]. In flies, it is in fact not clear if they can at all sense body orientation in an absolute sense [35,36], while the sensing of rotational velocity by the visual system (for a review, see [37]) and the halteres [17–19] is very evident.

In the nested control loop shown in figure 1, visual and mechanosensory feedback play complementary roles. The visual loop provides the external reference to set the ground speed [6,7,38] with comparably slow response properties [9,11,39]. In contrast, the mechanosensory loop provides extremely fast [18,40,41] proprioceptive feedback to control pitch, which is inherently unstable [30,42]. Additional visual input is also present to control pitch at lower frequencies [19].

As an emergent property of the nested control structure, this system provides an automatic drift compensation mechanism. An error in the pitch integrator, for example, would propagate to the body pitch angle, and next flight speed. This error would be sensed by the visual system and be compensated by adjusting the pitch angle set point.

Similarly, a change of wind speed would simply be compensated by an adjustment of the pitch set point value. This mechanism is likely to be general to flying insects, in which wind speed compensation is ubiquitous (*Aedes* [3]; *Drosophila* [6,7]; *Apis* [43]). Owing to the linearity of the system, the control dynamics around the floating set point remain unaffected.

In conclusion, the linear plant provides the basis for a two-level nested controller requiring only two inputs. (i) Translational optic flow provides a visual reference signal to control the ground speed. (ii) Mechanosensory feedback from the halteres signals the body rotational velocity. Because drift is compensated in the visual feedback loop, the system is robust for imperfect integration at the level of pitch angle computation, as could result, for example, from a leaky integration of the angular velocity. All these beneficial properties of the speed control system depend critically on the linearity of the pitch-to-speed transfer function.

4.2. The importance of wing damping

The identified linear relationship between the body pitch angle and air speed is consistent with previous results obtained in *Drosophila hydei* under steady-state conditions [13]. The linear dependence of body pitch and flight speed (measured at steady state) was attributed to opposing effects of a squared increase of body drag with air speed and a reduced projected area as the fly pitches nose down to increase flight speed. We instead find that body drag provides little damping compared with the flapping wings (figure 5*a*,*b*).

Analogous to the wing damping we measured for the speed responses, the wings of fruitflies provide substantial passive damping during the saccadic turning manoeuvres [24,32,44], while body drag is comparatively

insignificant [45]. Lacking detailed wing kinematics, we cannot exclude the possibility that the fly additionally adjusts them at increasing air speeds to maintain the measured linear relationship between body angle and flight speed [16]. Detailed measurements of wing kinematics are therefore required to assess the degree to which the fly actively tunes its linear speed damping. This approach would have to be followed through with a dynamically scaled wing model [46] or computational fluid dynamics [47] to capture the significant unsteady effects that are expected to arise at elevated advance ratios [28]. An analogous approach was taken in a recent study on the hawkmoth *Manduca sexta*, in which a combination of passive open-loop dynamics and feedback control was revealed [48]. By combining theory, modelling and behavioural studies within an integrative framework further progress can be made in our understanding of insect flight control mechanisms.

4.3. Embodied linearity

Recent behavioural studies have revealed that important visual flight control reflexes are organized within a linear control framework [9,11,49]. Such linearity is likely to have evolved due to selective advantages, such as the ability to operate on differential sensory inputs or to compensate drift efficiently. In the present case, we can show that this linearity emerges already at the level of the myogenic wing actuation mechanism and direct wing control reflexes.

The embodyment of suitable control properties in the low-level physiology may provide a quite general mechanism that provides high robustness and efficiency to demanding neuromotor control problems. These mechanisms may also provide design principles for MAVs, which underlie similarly severe performance constraints as flying insects. These are expected to be applicable also at the much larger scale, at which MAVs are currently being realized. Specifically, the linear damping resulting from flapping wings is related to a turbulent flow regime characteristic for high Reynolds numbers [32], and is therefore expected to apply similarly in larger flapping MAVs. More generally even, the embodiment of linear properties in the low-level actuation mechanisms may represent an important principle in entirely different animal locomotion systems and be relevant to various biorobotic applications.

V.M. was supported by the Swiss National Science Foundation (CR23I2_125419/1) and the Volkswagen Foundation (I/80 984–986). S.N.F. was supported by the Human Frontier Science Program (RGP25/2006). We thank Chauncey Graetzel and Nicola Rohrseitz for helping with the experimental design and for useful discussions.

APPENDIX A. BODY DRAG ESTIMATE

Body drag was calculated as a function of air speed and pitch angle according to a model proposed by Dickson *et al.* [22]. Parallel (F_P) and normal (F_N) aerodynamic force components with respect to the body long axis are calculated as follows:

$$F_P = \frac{1}{2}\rho C_P(\delta) S \|\boldsymbol{u}_b\|^2 \quad (A\,1)$$

and

$$F_N = \frac{1}{2}\rho C_N(\delta) S \|\boldsymbol{u}_b\|^2, \quad (A\,2)$$

where ρ is the air density, S the body reference area, $\boldsymbol{u}_b$ the incident air velocity vector, δ the angle between the body longitudinal axis and the incident flow, and C_P, C_N the experimentally determined force coefficients. The coefficients are calculated from

$$C_P = k_P \cos\delta \quad \text{and} \quad C_N = k_N \sin\delta, \quad (A\,3)$$

where $k_P = 0.6$ and $k_N = 1.2$ in the case of *D. melanogaster* [22]. The horizontal and vertical components of the aerodynamic force acting on the body can be calculated from

$$F_{BD} = \cos(\theta) F_P + \sin(\theta) F_N \quad (A\,4)$$

and

$$F_{BL} = -\sin(\theta) F_P + \cos(\theta) F_N. \quad (A\,5)$$

The body accelerations for drag and lift as a function of the pitch angle and the air speed, calculated according to equations (A 1)–(A 5), are shown in the electronic supplementary material, figure S1*a*,*b*.

REFERENCES

1 Collett, T., Nalbach, H. O. & Wagner, H. 1993 Visual stabilization in arthropods. *Rev. Oculomot. Res.* **5**, 239–263.
2 Srinivasan, M. V. & Zhang, S. 2004 Visual motor computations in insects. *Annu. Rev. Neurosci.* **27**, 679–696. (doi:10.1146/annurev.neuro.27.070203.144343)
3 Kennedy, J. S. 1940 The visual responses of flying mosquitoes. *Proc. Zool. Soc. Lond. A* **109**, 221–242. (doi:10.1111/j.1096-3642.1940.tb00831.x)
4 Srinivasan, M. V., Lehrer, M., Kirchner, W. & Zhang, S. 1991 Range perception through apparent image speed in freely flying honeybees. *Visual Neurosci.* **6**, 519–535. (doi:10.1017/S095252380000136X)
5 Baird, E., Srinivasan, M. V., Zhang, S. & Cowling, A. 2005 Visual control of flight speed in honeybees. *J. Exp. Biol.* **208**, 3895–3905. (doi:10.1242/jeb.01818)
6 David, C. 1982 Compensation for height in the control of groundspeed by *Drosophila* in a new 'barber's pole' wind tunnel. *J. Comp. Physiol. A* **147**, 485–493. (doi:10.1007/BF00612014)
7 Fry, S. N., Rohrseitz, N., Straw, A. D. & Dickinson, M. H. 2009 Visual control of flight speed in *Drosophila melanogaster*. *J. Exp. Biol.* **212**, 1120–1130. (doi:10.1242/jeb.020768)
8 Fry, S. N., Rohrseitz, N., Straw, A. D. & Dickinson, M. H. 2008 TrackFly: virtual reality for a behavioral system analysis in free-flying fruit flies. *J. Neurosci. Methods* **171**, 110–117. (doi:10.1016/j.jneumeth.2008.02.016)
9 Rohrseitz, N. & Fry, S. N. 2010 Behavioural system identification of visual flight speed control in *Drosophila melanogaster*. *J. R. Soc. Interface* **8**, 171–185. (doi:10.1098/rsif.2010.0225)
10 David, C. 1984 The dynamics of height stabilization in *Drosophila*. *Physiol. Entomol.* **9**, 377–386. (doi:10.1111/j.1365-3032.1984.tb00778.x)

11 Graetzel, C. F., Nelson, B. J. & Fry, S. N. 2010 Frequency response of lift control in *Drosophila*. *J. R. Soc. Interface* **7**, 1603–1616. (doi:10.1098/rsif.2010.0040)
12 Vogel, S. 1966 Flight in *Drosophila*. I. Flight performance of tethered flies. *J. Exp. Biol.* **44**, 567–578.
13 David, C. T. 1978 The relationship between body angle and flight speed in free-flying *Drosophila*. *Physiol. Entomol.* **3**, 191–195. (doi:10.1111/j.1365-3032.1978.tb00148.x)
14 Fry, S. N., Sayaman, R. & Dickinson, M. H. 2005 The aerodynamics of hovering flight in *Drosophila*. *J. Exp. Biol.* **208**, 2303–2318. (doi:10.1242/jeb.01612)
15 Götz, K. G. 1968 Flight control in *Drosophila* by visual perception of motion. *Biol. Cybern.* **4**, 199–208.
16 Ristroph, L., Bergou, A. J., Guckenheimer, J., Wang, Z. J. & Cohen, I. 2011 Paddling mode of forward flight in insects. *Phys. Rev. Lett.* **106**, 178103. (doi:10.1103/PhysRevLett.106.178103)
17 Pringle, J. W. S. 1948 The gyroscopic mechanism of the halteres of Diptera. *Phil. Trans. R. Soc. Lond. B* **233**, 347–384. (doi:10.1098/rstb.1948.0007)
18 Nalbach, G. & Hengstenberg, R. 1994 The halteres of the blowfly *Calliphora*. II. Three-dimensional organisation of compensatory reactions to real and simulated rotations. *J. Comp. Physiol. A* **175**, 695–708. (doi:10.1007/BF00191842)
19 Sherman, A. & Dickinson, M. H. 2004 Summation of visual and mechanosensory feedback in *Drosophila* flight control. *J. Exp. Biol.* **207**, 133–142. (doi:10.1242/jeb.00731)
20 Taylor, G. K. 2001 Mechanics and aerodynamics of insect flight control. *Biol. Rev.* **76**, 449–471. (doi:10.1017/S1464793101005759)
21 Reiser, M. B., Humbert, J. S., Dunlop, M. J., Del Vecchio, D., Murray, R. M. & Dickinson, M. H. 2004 Vision as a compensatory mechanism for disturbance rejection in upwind flight. In *Proc. American Control Conf.,* vol. 1, pp. 311–316. See http://ieeexplore.ieee.org/xpls/abs_all.jsp?arnumber=1383623)
22 Dickson, W. B., Straw, A. D. & Dickinson, M. H. 2008 Integrative model of *Drosophila* flight. *AIAA J.* **46**, 2150–2164. (doi:10.2514/1.29862)
23 Farina, W., Kramer, D. & Varjú, D. 1995 The response of the hovering hawk moth *Macroglossum stellatarum* to translatory pattern motion. *J. Comp. Physiol. A* **176**, 551–562. (doi:10.1007/BF00196420)
24 Cheng, B., Fry, S. N., Huang, Q. & Deng, X. 2010 Aerodynamic damping during rapid flight maneuvers in the fruit fly *Drosophila*. *J. Exp. Biol.* **213**, 602–612. (doi:10.1242/jeb.038778)
25 Robert, D., Fry, S. N., Müller, P., Baumann, H.-J., Straw, A. D. & Bichsel, M. 2004 Context-dependent stimulus presentation to freely moving animals in 3D. *J. Neurosci. Methods* **135**, 149–157. (doi:10.1016/j.jneumeth.2003.12.012)
26 Straw, A. D. & O'Carroll, D. C. 2003 Motion blur applied to eliminate artifacts in apparent motion displays. *J. Vis.* **3**, 782. (doi:10.1167/3.9.782)
27 Graetzel, C. F., Fry, S. N. & Nelson, B. J. 2006 A 6000 Hz computer vision system for real-time wing beat analysis of *Drosophila*. In *1st IEEE RAS and EMBS Int. Conf. on Biomedical Robotics and Biomechatronics* (*BioRob 2006*), pp. 278–283. (doi:10.1109/BIOROB.2006.1639099)
28 Dickson, W. B. & Dickinson, M. H. 2004 The effect of advance ratio on the aerodynamics of revolving wings. *J. Exp. Biol.* **207**, 4269–4281. (doi:10.1242/jeb.01266)
29 Ellington, C. P. 1984 The aerodynamics of hovering insect flight. III. Kinematics. *Phil. Trans. R. Soc. Lond. B* **305**, 41–78. (doi:10.1098/rstb.1984.0051)
30 Cheng, B. & Deng, X. 2011 Translational and rotational damping of flapping flight and its dynamics and stability at hovering. *IEEE Trans. Robot.* **27**, 849–864. (doi:10.1109/TRO.2011.2156170)
31 Faruque, I. & Sean Humbert, J. 2010 Dipteran insect flight dynamics. I. Longitudinal motion about hover. *J. Theor. Biol.* **264**, 538–552. (doi:10.1016/j.jtbi.2010.02.018)
32 Hedrick, T. L., Cheng, B. & Deng, X. 2009 Wingbeat time and the scaling of passive rotational damping in flapping flight. *Science* **324**, 252–255. (doi:10.1126/science.1168431)
33 Marden, J. H., Wolf, M. R. & Weber, K. E. 1997 Aerial performance of *Drosophila melanogaster* from populations selected for upwind flight ability. *J. Exp. Biol.* **200**, 2747–2755.
34 Taylor, G. K. & Krapp, H. G. 2007 Sensory systems and flight stability: what do insects measure and why? In *Insect mechanics and control 34* (eds J. Casas & S. J. Simpson), pp. 231–316. New York, NY: Academic Press.
35 Hengstenberg, R. 1988 Mechanosensory control of compensatory head roll during flight in the blowfly *Calliphora erythrocephala* Meig. *J. Comp. Physiol. A* **163**, 151–165. (doi:10.1007/BF00612425)
36 Srinivasan, M. V. 1977 A visually-evoked roll response in the housefly. *J. Comp. Physiol. A* **119**, 1–14. (doi:10.1007/BF00655868)
37 Hausen, K. 1993 Decoding of retinal image flow in insects. *Rev. Oculomot. Res.* **5**, 203–235.
38 Srinivasan, M. V., Zhang, S., Lehrer, M. & Collett, T. S. 1996 Honeybee navigation en route to the goal: visual flight control and odometry. *J. Exp. Biol.* **199**, 237–244.
39 Heisenberg, M. & Wolf, R. 1993 The sensory-motor link in motion-dependent flight control of flies. *Rev. Oculomot. Res.* **5**, 265–283.
40 Sandeman, D. C. & Markl, H. 1980 Head movements in flies (*Calliphora*) produced by deflexion of the halteres. *J. Exp. Biol.* **85**, 43–60.
41 Ristroph, L., Bergou, A. J., Ristroph, G., Coumes, K., Berman, G. J., Guckenheimer, J., Wang, Z. J. & Cohen, I. 2010 Discovering the flight autostabilizer of fruit flies by inducing aerial stumbles. *Proc. Natl Acad. Sci. USA* **107**, 4820–4824. (doi:10.1073/pnas.1000615107)
42 Sun, M., Wang, J. & Xiong, Y. 2007 Dynamic flight stability of hovering insects. *Acta Mech. Sinica* **23**, 231–246. (doi:10.1007/s10409-007-0068-3)
43 Barron, A. & Srinivasan, M. V. 2006 Visual regulation of ground speed and headwind compensation in freely flying honey bees (*Apis mellifera* L.). *J. Exp. Biol.* **209**, 978–984. (doi:10.1242/jeb.02085)
44 Hesselberg, T. & Lehmann, F.-O. 2007 Turning behaviour depends on frictional damping in the fruit fly *Drosophila*. *J. Exp. Biol.* **210**, 4319–4334. (doi:10.1242/jeb.010389)
45 Fry, S. N., Sayaman, R. & Dickinson, M. H. 2003 The aerodynamics of free-flight maneuvers in *Drosophila*. *Science* **300**, 495–498. (doi:10.1126/science.1081944)
46 Sane, S. P. & Dickinson, M. H. 2001 The control of flight force by a flapping wing: lift and drag production. *J. Exp. Biol.* **204**, 2607–2626.
47 Wang, Z. J. 2005 Dissecting insect flight. *Annu. Rev. Fluid Mech.* **37**, 183–210. (doi:10.1146/annurev.fluid.36.050802.121940)
48 Cheng, B., Deng, X. & Hedrick, T. L. 2011 The mechanics and control of pitching manoeuvres in a freely flying hawkmoth (*Manduca sexta*). *J. Exp. Biol.* **214**, 4092–4106. (doi:10.1242/jeb.062760)
49 Theobald, J. C., Ringach, D. L. & Frye, M. A. 2010 Dynamics of optomotor responses in *Drosophila* to perturbations in optic flow. *J. Exp. Biol.* **213**, 1366–1375. (doi:10.1242/jeb.037945)